COBEM 2023 27TH INTERNATIONAL CONGRESS OF MECHANICAL ENGENEERING

ABCM Brazilian Society of Mechanical Sciences and Engineering
27th ABCM International Congress of Mechanical Engineering
December 04-08, 2023, Florianópolis-SC, Brazil

COB-2023-0124
A STUDY ON THE RAYLEIGH WAVE ATTENUATION PROVIDED BY GABION MATS USING A COUPLED IBEM-FEM MODEL

L. A. Marques

School of Mechanical Engineering, University of Campinas. 200 Mendeleyev St, Campinas SP Brazil

l201083@dac.unicamp.br

D. Carneiro

KU Leuven, Dept. of Civil Eng., Structural Mechanics Section, Kasteelpark Arenberg 40 box 2448, B-3001 Leuven, Belgium

david.carneiro@kuleuven.be

J. Labaki

School of Mechanical Engineering, University of Campinas. 200 Mendeleyev St, Campinas SP Brazil

labaki@unicamp.br

Abstract. *This article presents a study on ground vibration attenuation induced by flat surface structures, such as gabion mats and concrete slabs. The objective of this research is to understand the mechanisms of attenuation that surface structures of different dimensions and constitutive properties are able to provide and also find optimal configurations for maximum vibration attenuation. Railway traffic and busy roadways are important sources of ground vibration, which can lead to disturbances in the lives of people who live near them. Understanding how this unwanted vibration can be reduced is key to improve life quality and also an example of practical benefit that can be achieved from this study. The materials used in the analyses are designed to reduce the construction cost of protection against ground vibration, since they are relatively inexpensive to build and to maintain. The analyses consider ground vibration resulting from seismic excitation in the form of plane Rayleigh waves and from a harmonic source applied on the soil surface. A coupled Indirect Boundary Element Method - Finite Element Method (IBEM-FEM) model is used for the study, in which surface mats are modeled via classical finite elements, and the response of the soil is modeled via superposition of soil influence functions, within an IBEM framework. Coupling between the two subsystems is obtained by imposing continuity and equilibrium conditions on the soil-mat interface. The dynamic response of the coupled system is derived in the frequency domain, in which the coupled equations of motion can be solved algebraically. The paper discusses the mechanisms by which the vibration attenuation occurs comparing them to previous studies, as well as the similarities and differences between the vibration attenuation performance of surface plates and walls. Selected numerical results for various constitutive parameters are presented, which show that gabion mats may be an effective measure against ground vibration.*

Keywords: *Ground vibration attenuation, Soil-Structure Interaction, Coupled methods, Gabion mats.*

1. INTRODUCTION

Ground vibration has remarkable impact on the stability of both surface and buried structures. Vibration-sensitive structures, such as particle accelerators and nuclear powerplants, have very strict limits on how much their foundations are allowed to vibrate in order to prevent improper operation and safety issues in installations like these. Ground vibration can originate from different sources, e.g. road and railway traffic or earthquakes, and the relevant frequency range for large-scale structures like those typically falls under 100 Hz.

Throughout the years, various engineering solutions against ground vibration have been studied. Casablanca *et al.* (2018) presented an approach based on designing sophisticated foundations that can counteract ground vibration. Kaewunruen *et al.* (2017) presented an approach that proposes to attenuate vibrations directly at the source by using absorptive

materials. A third class relies on installing some vibration-attenuation or vibration-blocking device on the propagation path between the vibration source and the target structure. These include open and filled trenches (Herbut, 2020; Bose *et al.*, 2018), elastic bodies such as piles and plates (Álamo *et al.*, 2019; Albino *et al.*, 2019), locally-resonant artificial or natural bodies (Colombi *et al.*, 2016), and surface structures (Krylov, 2007), which are the object of the present paper.

This work is inspired by the proposition by that decorative roadside boulders have a role on the vibration level that propagates from the road to its surroundings (Krylov, 2007). He showed that the mechanism by which boulders affect ground vibration is the scattering of Rayleigh waves into body waves projected into the bulk of the soil, and hence, reducing the amount of energy that propagates on the surface of the soil. Mhanna *et al.* (2014) and Masoumi *et al.* (2014) provided experimental evidence supporting this phenomenon, using water tanks and concrete blocks, respectively. These results separately investigated the effect of mass and stiffness on the vibration performance of these surface structures. Dijckmans *et al.* (2015) performed extensive parametric studies to further understand the performance of heavy surface walls, and argued that the attenuation performance of gabion and concrete walls are independently related to their horizontal, rocking, and flexural modes. More recently, Carneiro *et al.* (2022) put forward a coupled model involving the Indirect Boundary Element Method (IBEM) to represent the soil and the classical Finite Element Method (FEM) to represent the surface structure. With this IBEM-FEM coupling model, they were able to look more closely into the mechanism of conversion from surface to body waves by surface walls. They showed that wider walls do not necessarily provide better attenuation performance, and that the anisotropy of the soil is irrelevant to the attenuation performance of the wall. Auersch (2013) and Sanitate and Talbot (2019) investigated the effects of wider and thinner structures on the attenuation of ground vibration by using foundation slabs models. Both studies concluded that the most relevant parameter on the vibration attenuation level is the stiffness relation between soil and slab.

This work investigates the vibration attenuation provided by wide flat surface structures, referred here as "mats", and the mechanism by which the attenuation occurs. The model consists of the superposition of non-singular influence functions to represent the response of the soil, in the sense of an IBEM framework, together with the classical FEM to represent the response of the flat structure. Coupling between the two models is achieved in the frequency domain by imposing continuity and equilibrium conditions at the mat-soil interface. This condition results in an algebraic system of equations in the frequency domain, which can be solved for arbitrary frequencies of excitation. The effectiveness of the mats is studied by means of the computed responses beneath and behind the structure. The problem consists in comparing the vibration without and with the structure. The paper shows selected numerical results on the attenuation performance of flat structures with different geometric and constitutive parameters, and considers plane Rayleigh wave and harmonic surface load as excitation sources.

2. PROBLEM STATEMENT

The problem consists of a linear-elastic flat structure resting over the surface of the soil, which is modeled as a linear-elastic, homogeneous, isotropic, unbounded medium (Fig. 1). The contact interface between structure and soil is perfectly bounded. A flat structure of width L and thickness H is considered with Young's modulus E_m, Poisson ratio ν_m, and mass density ρ_m. The soil has Young's modulus E, Poisson ratio ν, and mass density ρ. Ground vibration can originate from plane Rayleigh waves or time-harmonic line loads applied on the surface of the soil. Because of the comparatively long length of the flat structure in practical applications, the problem is modeled as a 2D, plane-strain problem.

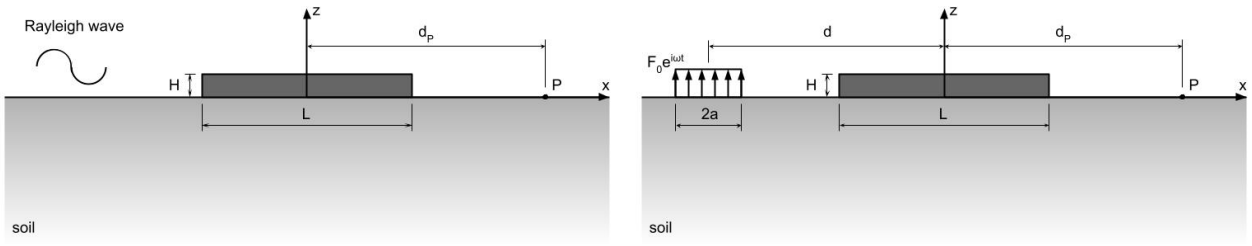

(a) (b)

Figure 1. Flat surface structure with (a) Rayleigh wave and (b) harmonic line load excitation considered in this work.

3. FORMULATION

3.1 Soil model

Consider a two-dimensional, transversely isotropic, homogeneous half-space, defined by four independent constitutive parameters c_{11}, c_{13}, c_{33} and c_{44}, and mass density ρ, subjected to time-harmonic excitation of circular frequency ω. Rajapakse and Wang (1991) derived the following solutions for the horizontal and vertical displacement fields in this

medium.

$$u_{xx} = -\frac{2}{\pi c_{44}\delta}\int_0^\infty \frac{1}{R}\left(\eta_3\bar{\omega}_1 e^{\delta\xi_1 z} - \eta_4\bar{\omega}_2 e^{\delta\xi_2 z}\right)\cos\left(\delta\zeta x\right)d\zeta, \tag{1}$$

$$u_{zx} = -\frac{2i}{\pi c_{44}\delta}\int_0^\infty \frac{1}{R}\left(\eta_3\bar{\omega}_1 e^{\delta\xi_1 z} - \eta_4\bar{\omega}_2 e^{\delta\xi_2 z}\right)\sin\left(\delta\zeta x\right)d\zeta, \tag{2}$$

$$u_{xz} = \frac{2i}{\pi c_{44}\delta}\int_0^\infty \frac{1}{R}\left(\eta_2\bar{\omega}_1 e^{\delta\xi_1 z} - \eta_1\bar{\omega}_2 e^{\delta\xi_2 z}\right)\sin\left(\delta\zeta x\right)d\zeta, \tag{3}$$

$$u_{zz} = \frac{2}{\pi c_{44}\delta}\int_0^\infty \frac{1}{R}\left(\eta_2\bar{\omega}_1 e^{\delta\xi_1 z} - \eta_1\bar{\omega}_2 e^{\delta\xi_2 z}\right)\cos\left(\delta\zeta x\right)d\zeta, \tag{4}$$

in which u_{ij} denotes displacement in the i-direction due to loads in the j-direction, $\zeta = \lambda/\delta$, $\alpha = c_{33}/c_{44}$, $\beta = c_{11}/c_{44}$, $\kappa = 1 + c_{13}/c_{44}$, $\delta^2 = \rho\omega^2/c_{44}$, and

$$R = \frac{\eta_1\eta_3 - \eta_2\eta_4}{\sin\left(\delta\zeta a\right)}\zeta, \tag{5}$$

$$\xi_{1,2}^2 = \left(\gamma\zeta^2 - 1 - \alpha \pm \sqrt{\Phi}\right)/\left(2\alpha\right), \tag{6}$$

$$\Phi = \left(\gamma\zeta^2 - 1 - \alpha\right)^2 - 4\alpha\left[\beta\zeta^4 - (1+\beta)\zeta^2 + 1\right], \tag{7}$$

$$\gamma = 1 + \alpha\beta - \kappa^2, \tag{8}$$

$$\bar{\omega}_i = \left(\alpha\xi_i^2 - \zeta^2 + 1\right)/-\left(i\kappa\zeta\xi_i\right), \tag{9}$$

$$\eta_{1,2} = -\xi_{1,2}\bar{\omega}_{1,2} + i\zeta, \tag{10}$$

and

$$\eta_{3,4} = (\kappa - 1)i\zeta\bar{\omega}_{2,1} - \alpha\xi_{2,1}. \tag{11}$$

The present case of an isotropic half-space, due to the 2D plane-strain model considered, is a particular case of the above, where

$$c_{11} = c_{33} = \frac{E(1-\nu)}{(1+\nu)(1-2\nu)}, \tag{12}$$

$$c_{12} = c_{13} = \frac{E\nu}{(1+\nu)(1-2\nu)}, \tag{13}$$

and

$$c_{44} = G = \frac{E}{2(1+\nu)}, \tag{14}$$

in which G is the shear modulus. A detailed description of the strategy used in this paper for the numerical evaluation of Eq. (1) to Eq. (4) is presented in Labaki *et al.* (2012).

3.2 IBEM-FEM model

In this paper, we use four-noded quadrilateral classical finite elements, which have two displacement degrees per node, to model the response of the surface structure. The equation of motion is given by

$$\bar{\mathbf{K}}\mathbf{u} = \mathbf{f}, \tag{15}$$

in which $\bar{\mathbf{K}} = \mathbf{K} - \omega^2\mathbf{M}$ is the dynamic stiffness matrix of the structure, and $\mathbf{u}$ and $\mathbf{f}$ are the vectors of displacement and forces at the nodes (Bathe, 2006).

The coupling between the soil and the structure can be represented by the inclusion of interface forces $\mathbf{f_s}$ that arise at the bottom of the structure due to the presence of the soil. The modified equation of motion for the nodes at the interface can be written as

$$\bar{\mathbf{K}}'\mathbf{u}' = \mathbf{f}' - \mathbf{f_s}, \tag{16}$$

where $\bar{\mathbf{K}}'$, $\mathbf{u}'$ and $\mathbf{f}'$ are, respectively, the dynamic stiffness matrix, structural displacement vector and force vector on the interface nodes.

The distribution of contact forces $\mathbf{f_s}$ experienced by the nodes of the structure must maintain equilibrium with the contact tractions experienced by the soil at the interface. This distribution is unknown, and can be approximated by piece-wise constant fictitious contact tractions $\mathbf{q}$, which are also unknown. The equilibrium condition between $\mathbf{f_s}$ and $\mathbf{q}$ can be stated as

$$\mathbf{f_s} = \mathbf{A}\mathbf{q}, \tag{17}$$

in which $\mathbf{A}$ is a purely geometric transformation matrix. Now, Eq. (16) can be rewritten as

$$\bar{\mathbf{K}}'\mathbf{u}' + \mathbf{A}\mathbf{q} = \mathbf{f}'. \tag{18}$$

This paper considers seismic excitation in the form of both Rayleigh waves and harmonic line load. Due to the presence of the flat surface structure, an incident seismic wave $\mathbf{s^{(i)}}$ is partially scattered into $\mathbf{s^{(s)}}$, so that the resulting displacement $\mathbf{w_s}$ at the mat-soil interface is the sum of these two parts as (Fairweather *et al.*, 2003)

$$\mathbf{w_s} = \mathbf{s^{(i)}} + \mathbf{s^{(s)}}, \tag{19}$$

The scattered portion can be expressed in terms of the contact tractions $\mathbf{q}$ as

$$\mathbf{s^{(s)}} = \mathbf{U}\mathbf{q}, \tag{20}$$

in which $\mathbf{U}$ is the influence matrix of the soil, which terms come from Eq. (1) to Eq. (4). Displacements $\mathbf{w_s}$ can also be written in terms of the structural displacement $\mathbf{u}'$ at the interface as

$$\mathbf{w_s} = \mathbf{D}\mathbf{u}', \tag{21}$$

in which $\mathbf{D}$ is a purely geometric transformation matrix. Substituting Eqs. (20) and (21) into Eq. (19) yields:

$$\mathbf{D}\mathbf{u}' - \mathbf{U}\mathbf{q} = \mathbf{s^{(i)}}. \tag{22}$$

In this paper, $\mathbf{s^{(i)}}$ is both the incident Rayleigh wave and the displacements generated by the harmonic line load. For more details on matrices $\mathbf{A}$ and $\mathbf{D}$, the author is referred to Carneiro *et al.* (2022). The continuity condition expressed by Eq. (22) corresponds to the perfectly bonded contact between the structure and the soil, which is a reasonable hypothesis for the case of heavy structures and low frequency of excitation considered in this paper.

Combining Eqs. (18) and (22), and expanding the terms for the full system, yields:

$$\begin{bmatrix} \bar{\mathbf{K}} & \begin{bmatrix}\mathbf{0}\\ \mathbf{A}\end{bmatrix} \\ \begin{bmatrix}\mathbf{0} & \mathbf{D}\end{bmatrix} & -\mathbf{U} \end{bmatrix} \begin{Bmatrix} \mathbf{u} \\ \mathbf{q} \end{Bmatrix} = \begin{Bmatrix} \mathbf{0} \\ \mathbf{s^{(i)}} \end{Bmatrix}. \tag{23}$$

The incident seismic excitation $\mathbf{s^{(i)}}$ corresponding to Rayleigh waves of amplitude s_k in the k-direction ($k = x, z$) can be described as

$$\mathbf{s^{(i)}} = \{s_x \quad s_z\}^T e^{i(\omega t - k_R x)}, \tag{24}$$

in which $k_R = \omega/c_R$ is the Rayleigh wave number. The Rayleigh wave velocity c_R can be approximated from the shear wave speed $c_S = \sqrt{c_{44}/\rho}$ as (Haddad, 2012)

$$c_R = \frac{0.862 + 1.14\nu}{1 + \nu}, \tag{25}$$

in which ν is the Poisson ratio of the half-space. Additionally, s_x and s_z hold the following relation (Richart *et al.*, 1970):

$$s_x = ik_R S \left[e^{-k_P z} + 2\frac{k_P k_S}{k_S^2 + k_R^2} e^{-k_S z} \right], \tag{26}$$

and

$$s_z = -k_R S \left[\frac{k_P}{k_R} e^{-k_P z} + 2\frac{k_P k_R}{k_S^2 + k_R^2} e^{-k_R z} \right], \tag{27}$$

in which S is the absolute wave amplitude, and $k_{P,S}^2 = k_R^2 - \omega^2/c_{P,S}^2$, with c_P being the pressure wave speed.

4. NUMERICAL RESULTS

This section considers the time-harmonic response of the half-space, before and after the inclusion of a surface structure. These results consider a half-space and gabion mats of thickness $H = 0.5$ m and $H = 1.0$ m, and width $L = 5$ m, $L = 10$ m and $L = 20$ m, with the material properties shown in Tab. 1.

Table 1. Material properties of soil and flat structures considered in this study.

Medium	c_s **(m/s)**	c_p **(m/s)**	E **(MPa)**	ν	ρ **(kg/m^3)**	η
Soil	250	1470			1945	0.025
Gabion mat			367	0.2	1700	0.02

Results are measured at points of coordinates ($x = L/4$, $z = 0$) and ($x = 0$, $z = 0$) along the structure, and at a point P of coordinates ($x = 20$, $z = 0$) behind the structure on the soil. Figures 2 to 5 show selected numerical results on the attenuation performance of gabion mats on ground vibration induced by Rayleigh waves. These results are shown in terms of the attenuation ratio $Ar_{ij} = u_i^{(a)}/u_i^{(b)}$, in which $u_i^{(a)}$ and $u_i^{(b)}$ are the magnitudes of ground motion in the i-direction after and before the installation of the structure, respectively. Attenuation ratio values lower than 100% means that the presence of the gabion mat reduces the ground vibration. A dashed horizontal line has been included at $Ar_{ij} = 100\%$ mark in these graphs to facilitate the interpretation of the results.

Figures 2a and 2b show that there is no amplification of the horizontal motion beneath the structure and that wider mats can provide larger attenuation. Figure 2b shows a reduction of 97% of the magnitude of ground motion for the three mats considered at 60 Hz. Figure 2c shows an oscillatory behaviour of all curves in low frequencies, in which a maximum vibration amplification of 8.7% can be observed at 16 Hz for the widest mat, and a continuous increase on the attenuation performances can be seen for frequencies higher than 50 Hz, where a maximum vibration reduction of 45.7% is observed at 99 Hz. Increasing the thickness of the structure, Fig. 3a shows a peak of amplification that reaches an increase of 50% of the horizontal motion magnitude for the $L = 10$ m-mat. Figure 3b shows that the point of maximum attenuation observed at $x = L/4$ for the thinner mats (Fig. 2b) have moved to the left with the increase of the structure thickness (Fig. 3b), except for the narrower mat, which does not reach as large attenuation as the others. Figure 3c shows an increase on the rate in which the system achieve larger attenuation levels, reaching a reduction of 75.5% of the horizontal motion for the $L = 10$ m-mat at 97 Hz. The amplitude of oscillation at lower frequencies is larger in Fig. 3c, which leads to an amplification of 16.5% in the horizontal motion at 16 Hz for the widest mat. The increase of the mats thickness improves the attenuation performance of the gabion mat.

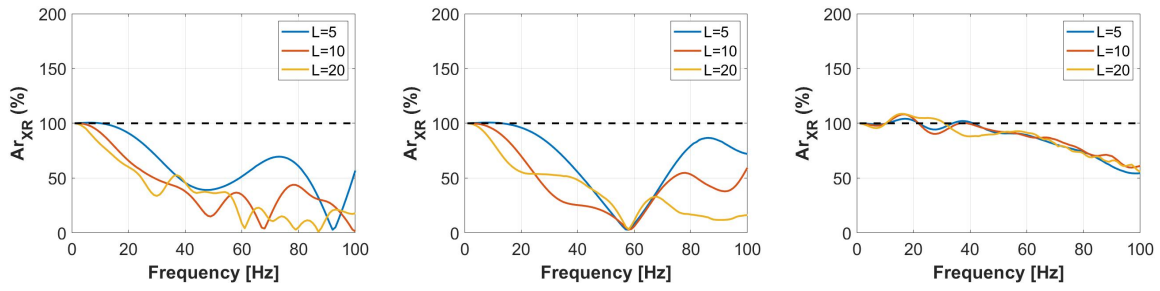

(a) (b) (c)

Figure 2. Attenuation ratio of horizontal vibration due to Rayleigh waves provided by flat structures of thickness $H = 0.5$ m at (a) $x = 0$, (b) $x = L/4$ and (c) $x = 20$ m.

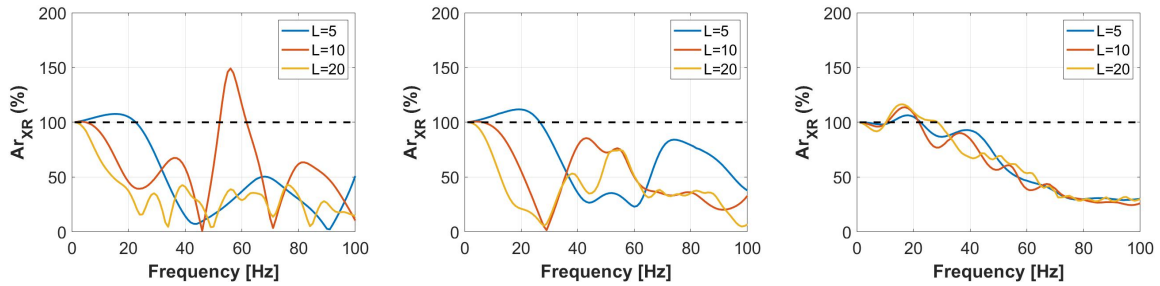

(a) (b) (c)

Figure 3. Attenuation ratio of horizontal vibration due to Rayleigh waves provided by flat structures of thickness $H = 1$ m at (a) $x = 0$, (b) $x = L/4$ and (c) $x = 20$ m.

Figures 4a and 4b show that, beneath the structure, amplification of the vertical motion is obtained for most of the excitation spectrum. In Fig. 4b it is straightforward to see that wider mats produce vibration amplification at lower frequencies and vibration attenuation at higher frequencies, while narrower mats produce amplification of ground motion at higher frequencies and no effects at lower frequencies. Figure 4c presents similar behavior compared to the horizontal displacement curves, except for the smaller oscillation amplitude in the attenuation ratio, which produces a maximum vibration amplification of 3.3% at 10 Hz for the $L = 20$ m-mat. Larger vibration attenuation levels can be obtained by increasing the thickness of the structure as shown in Figs. 5a and 5b. A comparison between Figs. 4c and 5c shows better vibration attenuation performance for thicker mats, where a maximum reduction of 75.6% of the vertical ground motion is observed at 97 Hz for the $L = 10$ m-mat and a maximum increase of 6.2% of the vertical vibration is observed at 10 Hz for the $L = 20$ m-mat. Similarly to the horizontal vibration (Figs. 2 and 3), an increase on the structure thickness has improved its vertical motion attenuation performance.

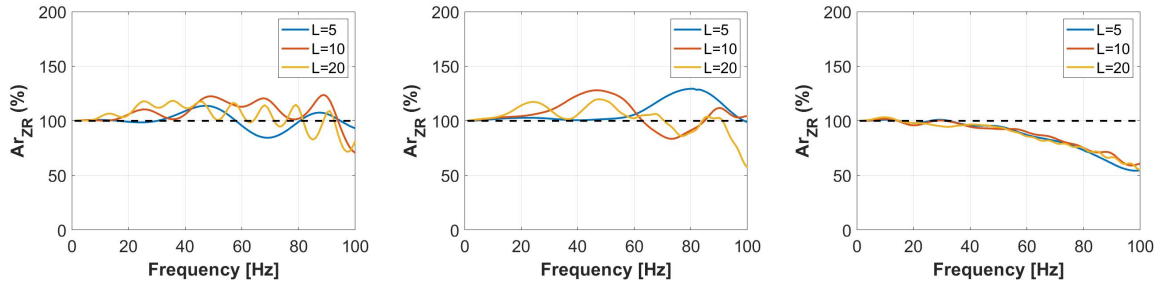

(a) (b) (c)

Figure 4. Attenuation ratio of vertical vibration due to Rayleigh waves provided by flat structures of thickness $H = 0.5$ m at (a) $x = 0$, (b) $x = L/4$ and (c) $x = 20$ m.

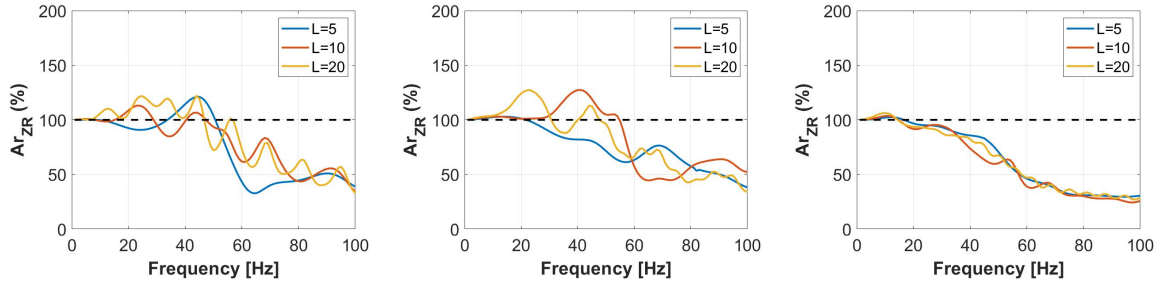

(a) (b) (c)

Figure 5. Attenuation ratio of vertical vibration due to Rayleigh waves provided by flat structures of thickness $H = 1$ m at (a) $x = 0$, (b) $x = L/4$ and (c) $x = 20$ m.

Figure 6 shows three frames of the harmonic wave propagation in the mat-soil system in different time steps. The color distribution indicates the longitudinal strain ε_{ZZ} propagating in the system, in which red represents positive strain and blue represents negative strain. The arrows labeled as "Structure Wavefront" and "Soil Wavefront" indicate the waves propagating in the gabion mat and in the soil, respectively. Note that, when going forward in time, the wavefronts in each medium start to move apart from each other, which is due to the different wave propagation velocity of each medium.

The wave propagation in the structure indicates that the attenuation mechanism of wider structures are not similar to the narrower ones. Narrow structures can be modeled as one-dimensional mass-spring resonators depending on how narrow they are compared to the wavelength and, as a consequence, the attenuation mechanism of the structure is related to vibration modes of the structure (Carneiro *et al.*, 2022). For wider structures, as gabion mats, one resonator is not enough to model the system as the structure is wider than the wavelength. This evokes more complex phenomena where there is no relation between the vibration modes and the vibration attenuation performance.

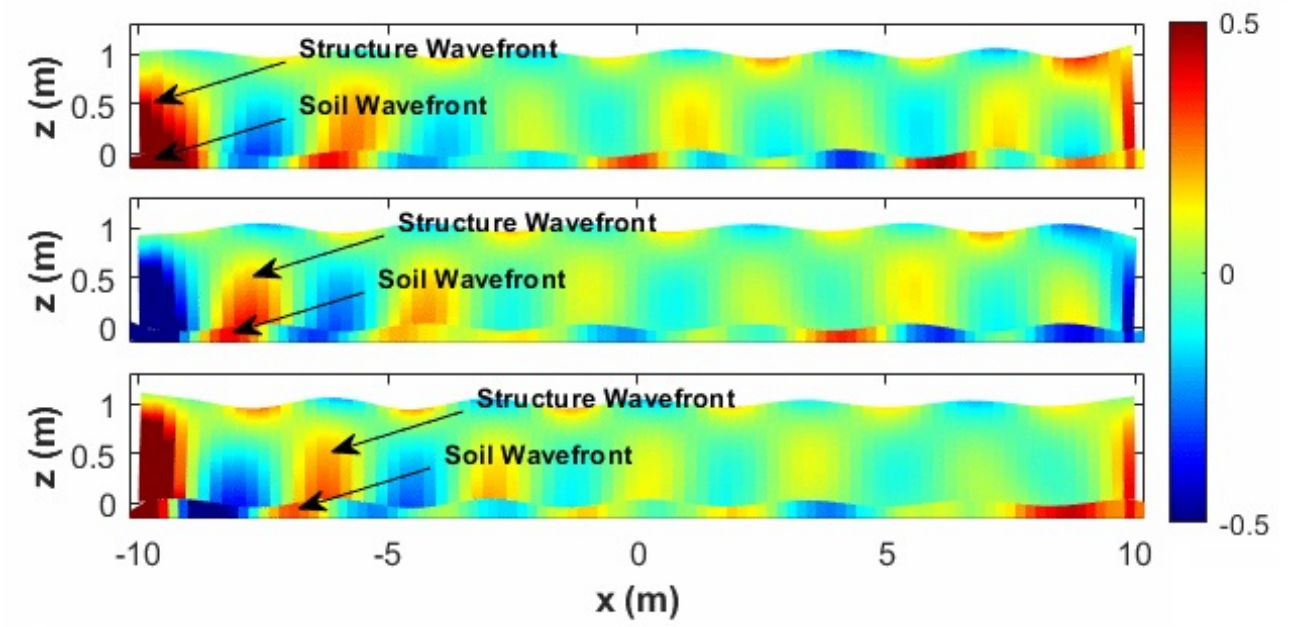

Figure 6. Wavefronts propagating in a gabion mat of thickness $H = 1$ m and width $L = 20$ m, and in the soil due to Rayleigh wave excitation of 80 Hz.

Figures 7 and 8 show the vertical displacements of the soil due to a vertical external line load applied 20 meters from the center of the structure ($d = 20$ m). This case is closer to reality as it considers material damping in the soil and body waves that are propagated towards the depth of the soil from the source. The results show that the attenuation performance of the gabion mats has slightly changed in comparison to the Rayleigh wave case (Figs. 4 and 5). At low frequencies along the structure, the points of maximum attenuation and amplification have changed, while at high frequencies the performances are almost the same. Figure 8c shows that, behind the mat, the attenuation performance is slightly worse along the entire spectrum, where an increase of 21.7% of vertical motion can be observed for the widest mat. Maximum reduction of 69.2% of the magnitude of the vertical motion is observed at 97 Hz for the widest and thickest mat (Fig. 8c).

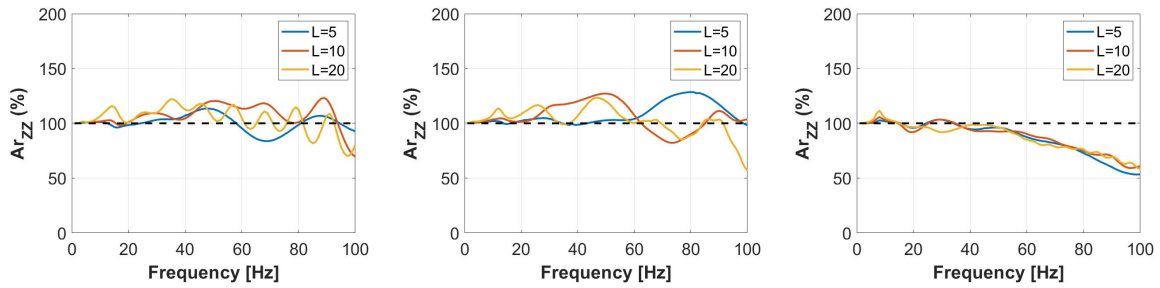

(a) (b) (c)

Figure 7. Attenuation ratio of vertical vibration due to vertical external load provided by flat structures of thickness $H = 0.5$ m at (a) $x = 0$, (b) $x = L/4$ and (c) $x = 20$ m.

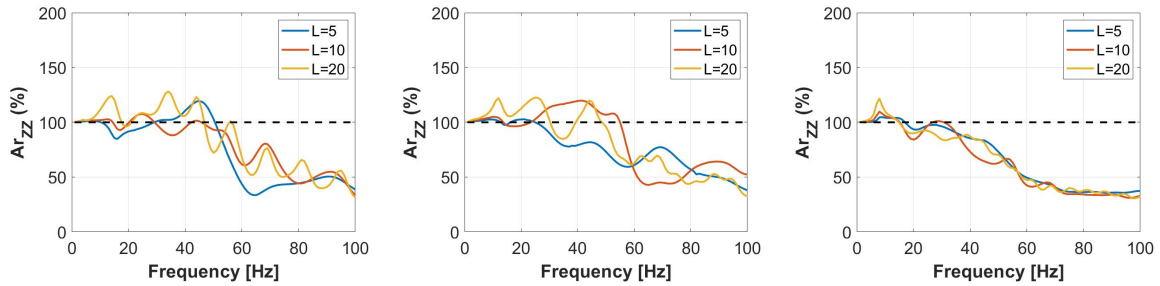

(a) (b) (c)

Figure 8. Attenuation ratio of vertical vibration due to vertical external load provided by flat structures of thickness $H = 1$ m at (a) $x = 0$, (b) $x = L/4$ and (c) $x = 20$ m.

5. CONCLUSION

This paper presented a study of the vibration attenuation performance of the flat surface structures to ground vibration. The model consisted of a coupled IBEM-FEM approach which allows an accurate representation of the wave propagation in homogeneous soils with the presence of surface structures. Gabion mats of different thickness and widths were considered. The results showed that gabion mats provides significant ground vibration attenuation at points beneath and behind the mat, indicating that these structures may be employed for attenuating train induced vibration. The increase of the structures thickness showed to improve their attenuation performances. No correlation was found between the mats widths and their vibration attenuation performances. The mechanism of attenuation of wider structures proved to be more complex than the narrower ones and is yet to be more explored and understood.

6. ACKNOWLEDGEMENTS

The research leading to this paper has been funded in part by the São Paulo Research Foundation (Fapesp) through grant number 2022/02753-5. The author D.C. acknowledges the Research Foundation Flanders (FWO Flanders) for the financial support obtained within the frame of the project G0B8221N “Mitigation of railway induced vibration using seismic metamaterials”.

7. REFERENCES

Álamo, G.M., Bordón, J.D., Aznarez, J.J. and Lombaert, G., 2019. “The effectiveness of a pile barrier for vibration transmission in a soil stratum over a rigid bedrock”. *Computers and Geotechnics*, Vol. 110, pp. 274–286.

Albino, C., Godinho, L., Amado Mendes, P., Alves Costa, P., Dias da Costa, D. and Soares Jr., D., 2019. “A technique based on adaptive extended jacobians for improving the robustness of the inverse numerical kinematics of redundant robots”. *Engineering Structures*, Vol. 196.

Auersch, L., 2013. “Response to harmonic wave excitation of finite or infinite elastic plates on a homogeneous or layered half-space”. *Computers and Geotechnics*, Vol. 51, pp. 50–59.

Bathe, K.J., 2006. *Finite element procedures*. Prentice Hall.

Bose, T., Choudhury, D., Sprengel, J. and Ziegler, M., 2018. “Efficiency of open and infill trenches in mitigating ground-borne vibrations”. *Journal of Geotechnical and Geoenvironmental Engineering*, Vol. 144(8).

Carneiro, D., Barros, P.L.A. and Labaki, J., 2022. “Ground vibration attenuation performance of surface walls”. *Computers and Geotechnics*, Vol. 149.

Casablanca, O., Ventura, G., Garesci, F., Azzerboni, B., Chiaia, B., Chippini, M. and Finocchio, G., 2018. “Seismic isolation of buildings using composite foundations based on metamaterials”. *Journal of Applied Physics*, Vol. 123.

Colombi, A., Roux, P., Guenneau, S., Gueguen, P. and Craster, R.V., 2016. “Forests as a natural seismic metamaterial: Rayleigh wave bandgaps induced by local resonances”. *Scientific reports*, Vol. 6.

Dijckmans, A., Coulier, P., Jiang, J., Toward, M., Thompson, D., Degrande, G. and Lombaert, G., 2015. “Mitigation of railway induced ground vibration by heavy masses next to the track”. *Soil Dynamics and Earthquake Engineering*, Vol. 75, pp. 158–170.

Fairweather, G., Karageorghis, A. and Martin, P.A., 2003. “The method of fundamental solutions for scattering and radiation problems”. *Engineering Analysis with Boundary Elements*, Vol. 27(7), pp. 759–769.

Haddad, Y.M., 2012. *Mechanical Behaviour of Engineering Materials: Volume 2: Dynamic Loading and Intelligent Material Systems*. Springer.

Herbut, A., 2020. “Vibration mitigation efficiency of an inclined, curved, open trench”. *Plos one*, Vol. 15(2).

Kaewunruen, S., Aikawa, A. and Remennikov, A.M., 2017. “Vibration attenuation at rail joints through under sleeper

pads". *Procedia Engineering*, Vol. 189, pp. 193–198.

Krylov, V.V., 2007. "Control of traffic-induced ground vibrations by placing heavy masses on the ground surface". *Journal of low frequency noise, vibration and active control*, Vol. 26, pp. 311–320.

Labaki, J., Romanini, E. and Mesquita, E., 2012. "Stationary dynamic displacement solutions for a rectangular load applied within a 3D viscoelastic isotropic full space - part II: Implementation, validation, and numerical results". *Mathematical Problems in Engineering*, Vol. 2012.

Masoumi, H., Van Leuven, A. and Urbaniak, S., 2014. "Mitigation of train induced vibrations by wave impeding blocks: numerical prediction and experimental validation". In *Proceedings of the 9th International Conference on Structural Dynamics - EURODYN 2014*. Porto, Portugal.

Mhanna, M., Shahrour, I., Sadek, M. and Dunez, P., 2014. "Efficiency of heavy mass technology in traffic vibration reduction: Experimental and numerical investigation". *Computers and Geotechnics*, Vol. 55, pp. 141–149.

Rajapakse, R. and Wang, Y., 1991. "Elastodynamic Green's functions of orthotropic half plane". *Journal of Engineering Mechanics*, Vol. 117(3), pp. 588–604.

Richart, F., Hall, J. and Woods, R., 1970. *Vibration of soil and foundations*. Prentice Hall, New York.

Sanitate, G. and Talbot, J.P., 2019. "On the plate-like and layer-like response of slab foundations to ground-borne vibration". *Computers and Geotechnics*, Vol. 114.

8. RESPONSIBILITY NOTICE

The authors are solely responsible for the printed material included in this paper.